

Optimal Delivery Scheduling and Charging of EVs in the Navigation of a City Map

Fernando V. Cerna, Mahdi Pourakbari-Kasmaei, *Member, IEEE*, Rubén A. Romero, *Senior Member, IEEE*, and Marcos J. Rider, *Senior Member, IEEE*

Abstract—This paper presents a mixed integer linear programming model to optimize the costs of maintenance and extra hours for scheduling a fleet of battery electric vehicles (BEVs) so that the products are delivered to prespecified delivery points along a route. On this route, each BEV must have an efficient charging strategy at the prespecified charging points. The proposed model considers the average speed of the BEVs, the battery states of charge, and a set of deliveries allocated to each BEV. The charging points are located on urban roads and differ according to their charging rate (fast or ultra-fast). Constraints that guarantee the performance of the fleet's batteries are also taken into consideration. Uncertainties in the navigation of urban roads are modeled using the probability of delay due to the presence of traffic signals, schools, and public works. The routes and the intersections of these routes are modeled as a predefined graph. The results and the evaluation of the model, with and without considering the extra hours, show the effectiveness of this type of transport technology. The models were implemented in AMPL and solved using the commercial solver CPLEX.

Index Terms—Battery electric vehicles, charging points, charging rates, mixed integer linear programming.

NOTATION

The notation used in this paper is presented as follows.

Sets

Ω_n	Set of intersections i .
Ω_a	Set of urban roads ki .
Ω_e	Set of deliveries e .
Ω_{vh}	Set of BEVs vh .

Parameters

δ^{km}	Costs for maintenance (R\$/km).
δ^{hx}	Costs for extra hours (R\$/h).

Manuscript received July 9, 2016; revised October 18, 2016 and January 12, 2017; accepted February 16, 2017. Date of publication February 22, 2017; date of current version August 21, 2018. This work was supported in part by the Brazilian Institution CNPq under Grant 141462/2013-2, and in part by the FAPESP under Grant 2014/22828-3 and Grant 2016/14319-7. Paper no. TSG-00915-2016.

F. V. Cerna, M. Pourakbari-Kasmaei, and R. A. Romero are with the Departamento de Engenharia Elétrica, Faculdade de Engenharia de Ilha Solteira, Universidade Estadual Paulista, Ilha Solteira 15385-000, Brazil (e-mail: fvcerna83@gmail.com; mahdi.pourakbari@ieee.org; ruben@dee.feis.unesp.br).

M. J. Rider is with the Department of Systems and Energy, School of Electrical and Computer Engineering, University of Campinas, Campinas 13083-852, Brazil (e-mail: mjrider@dsee.fee.unicamp.br).

Color versions of one or more of the figures in this paper are available online at <http://ieeexplore.ieee.org>.

Digital Object Identifier 10.1109/TSG.2017.2672801

$t_{vh,e,i}^n$	Type of intersection i in delivery of each BEV vh (-1: starting; 0: intermediate; 1: arrival).
d_{ki}	Length of urban road ki (km).
v_{vh}^{VE}	Average speed of BEV vh (km/h).
t^{max}	Total operating time (h).
τ^{PTS}	Delay time due to PTS (h).
τ^{PS}	Delay time due to PS (h).
τ^{PPW}	Delay time due to PPW (h).
P^{PTS}	Probability of delay due to PTS.
P^{PS}	Probability of delay due to PS.
P^{PPW}	Probability of delay due to PPW.
Δ_{ki}^{PTS}	Binary value that characterizes the occurrence of a delay due to PTS in urban road ki .
Δ_{ki}^{PS}	Binary value that characterizes the occurrence of a delay due to PS in urban road ki .
Δ_{ki}^{PPW}	Binary value that characterizes the occurrence of a delay due to PPW in urban road ki .
SOC_{vh}^o	Initial state of charge of the battery of BEV vh (kWh).
K^g	Energy spent during the navigation of BEV vh (kWh/km).
M	Big value used in the linearization process.
K^s	Storage capacity of the battery of BEV vh (kWh).
Y	Maximum number of discretizations of the variable $n_{vh,e,ki}^R$.
t_{ki}^a	Numerical value that characterizes the type of urban road ki (1: main road; 0: secondary road).
$\tau_{ki}^{MIN,UR}$	Minimum time for ultra-fast charging in urban road ki (h).
$\tau_{ki}^{MAX,UR}$	Maximum time for ultra-fast charging in urban road ki (h).
$\tau_{ki}^{MIN,R}$	Minimum time for fast charging in urban road ki (h).
$\tau_{ki}^{MAX,R}$	Maximum time for fast charging in urban road ki (h).
P_{ki}^{RU}	Unit charging rate in urban road ki (kW).
n_{ki}^P	Number of charging points in urban road ki .

Variables

$\omega_{vh,e,ki}$	Binary variable that indicates the navigation of BEV vh in urban road ki for delivery e .
$\varepsilon_{vh,e,ki}$	Total energy for charging the BEV vh in urban road ki for delivery e (kWh).

$SOC_{vh,e,i}^a$	Available state of charge of the battery of BEV vh at the moment of arrival at intersection i for delivery e (kWh).
$SOC_{vh,e,i}$	State of charge of the battery of BEV vh at intersection i for delivery e (kWh).
$\tau_{vh,e,ki}^{RU}$	Recharging time (for urban charging point available in road ki) for the battery of BEV vh for delivery e (h).
$n_{vh,e,ki}^R$	Number of charges made by BEV vh for delivery e in urban road ki .
Δt_{vh}	Extra hours related to BEV vh (h).
$\Delta''_{vh,e,ki}$	Continuous variable that represents the product of $\omega_{vh,e,ki}$ and $SOC_{vh,e,k}$ in the linearization process.
$W_{vh,e,ki,y}$	Binary variable used in the discretization $n_{vh,e,ki}^R$.
$\Delta W_{vh,e,ki,y}$	Continuous variable that represents the product of $\tau_{vh,e,ki}^{RU}$ and $W_{vh,e,ki,y}$ in the linearization process.
$\Delta Z_{vh,e,ki,y}$	Continuous variable that represents the product of $\Delta W_{vh,e,ki,y}$ and $\omega_{vh,e,ki}$ in the linearization process.

I. INTRODUCTION

THE DEVELOPMENT of less polluting technologies has become one of the most important targets for various sectors of industry. Among these, the transportation sector has sought to develop products that meet pollutant emission reduction targets and decrease the dependence on oil and its derivatives as energy sources [1]. In this context, electric vehicles (EVs) are presented as alternative transportation vehicles that are less pollutant and more efficient. Each EV's battery can be charged at a charging station connected to an electric network, which supplies propulsion for its mobility system [2]. The introduction of this technology and its several applications represents a great opportunity for synergy between the electricity and transport sectors. An important application of EVs is in the service sector, such as for product delivery, postal services, emergency services (police, ambulance), and so on. These services must ensure efficiency in deliveries by choosing the optimal route for each delivery while taking into account the battery state of charge, delay times in navigation, and charging at prespecified points located along the roads. Therefore, it is necessary to develop intelligent schemes to ensure the flexible navigation and efficient charging of EV fleets, considering time constraints, requirements, capacities, and so on [3].

In the literature, works related to the charging of BEVs in the navigation of a city map are scarce. In some works, the development of algorithms for routing with potential points of charging and optimal energy allocation has been considered [1], [2]. Another approach to optimal location of EV charging points was considered in [3]. This approach uses a fuzzy control to find the optimal location of charging points in an electrical distribution network, and takes into account the sensitivity indices obtained from the Newton-Raphson load flow assisting in the appropriate selection of charging point.

A methodology that aims at minimizing the total investment in a charging infrastructure and the cost for charging EVs was developed in [4]. This methodology was used to forecast the number of EVs to be charged at charging rates of slow, regular, and urgent. A cost reduction was also presented in [5]. This reduction is done in operating costs (energy and degradation of the battery costs) for a control model in the charging and discharging of the EV. Similarly, a control strategy for optimal charging of EVs was developed in [6]. The strategy considers the constraints related to the demand of EVs, a calculation algorithm of the total power for charging, and charging management for each EV. Moreover, a charging method of the EVs based on fuzzy control was implemented in [7]. In this method, the charging process is done by considering the deviation of the frequency of power distribution grid of IEEE 39 nodes with the presence of solar sources. The method implemented in MATLAB/SIMULINK environment takes into account: battery capacity, initial state of charge, initial charging time, etc.

Works related to the optimization of deliveries in service chains address this problem. In [8], a mixed-integer programming model that maximizes the profits by different delivery times for all consumers was proposed. The optimal scheduling of deliveries of products was addressed in [9] via fuzzy logic. This approach considers a number of situations between the driver's vehicle and each delivery to be done. Similarly, an integrated program delivery fleet that reduces carbon emissions by improving fleet efficiency and optimizing delivery times is developed in [10] and [11]. Some other works consider traffic information during the routing of vehicles. Thus, in [12] and [13], traffic information in real time was analyzed to determine optimal vehicle route. Based on this analysis, the decision-making processes that consider optimal routing policies, instant for the service, and simulation of vehicle flow using Markov processes are developed.

The problem of the shortest route was modeled in [14], which aimed to minimize charging costs along a route. This nonlinear model was modeled using dynamics programming for mono and multi vehicles. Another nonlinear model for minimizing navigation time and charging of an EV fleet was developed in [15]. An evolutionary genetic algorithm implemented in [16] aimed at determining the optimal routes for the navigation of fleets of EVs in order to minimize the costs associated with charging and operating time. Various models of the allocation of charging points in a city map have considered the density of traffic on urban roads throughout the day [17]–[20]. These works aimed to maximize the flow of EVs to be charged at the charging points. A heuristic algorithm that optimized the online service of charging points and considered time-dependent variable tariffs was proposed in [21] and extended in [22]. In [23], an online charging case was presented for managing a system of charging points. This online charging system was developed in Korea to optimize the charging of the mass transport system. Queuing theory was used in [24] to analyze the optimal management of charging stations, considering waiting rates and cost per service. Strategic scenarios were developed in [25]–[28], aiming to guarantee the optimal allocation of

charging points and to coordinate the management of EVs on the city map. The operation of the charging stations that maximized the operator's gains and the intelligent control of the charging rate at the stations supplied by solar energy was developed in [29] and [30], respectively. In [31] and [32], smart scheduling schemes were developed for charging and discharging EVs during the day in order to optimize the power charging so as to minimize the impact on the power grid by minimizing the costs associated with charging and discharging.

Moreover, the traditional optimization methods are not robust for facing dynamic changes and usually a complete restart must be provided to obtain a feasible solution (e.g., dynamic programming). In contrast, evolutionary algorithms are used in such changing circumstances. However, none of them can guarantee finding the optimal global solution [33].

This paper proposes an MILP model that aims to optimize the maintenance cost and cost of extra hours in the route scheduling of a BEV fleet in the navigation of a city map. In this optimization problem, the average speed, battery state of charge, and set of deliveries allocated to each available BEV in the fleet are considered. Moreover, charging points located along the roads, which are differentiated by charging rate (fast and ultra-fast), are taken into account. To guarantee the performance of the fleet's batteries, the corresponding constraints are applied. Uncertainties in the navigation of the city map are modeled using the probability of delays in the operation of the fleet due to PTS, PS, and PPW. To show the performance of the proposed approach, a city map containing roads and intersections was modeled as a graph of 71 nodes (intersections) and 131 edges (main and secondary roads). The analysis and evaluation of the proposed model, with and without considering the minimization of the extra hours of operation, showed promising results in the application of this type of transport technology. It should be noted that for both cases, the proposed model was implemented in AMPL language and the commercial solver CPLEX was used to find the optimal solution.

The main contributions of this paper are:

- An MILP model for the optimal route scheduling of EVs for charging during navigation considering prespecified delivery points that presents efficient computational behavior with conventional MILP solvers.
- A flexible model for analyzing the optimization of different scheduling strategies of EVs with consecutive deliveries so that they can be charged along their routes.
- The proposed model contributes a sustainable scenario in the use of energy resources, because toxic emissions in the city are minimized.

The remainder of this paper is structured as follows. In Section II, the hypotheses and uncertainties in the navigation are presented in detail. The mathematical formulation of an MINLP model and the linearization process are discussed in Section III. Section IV presents the case studies and results. Section V contains concluding remarks.

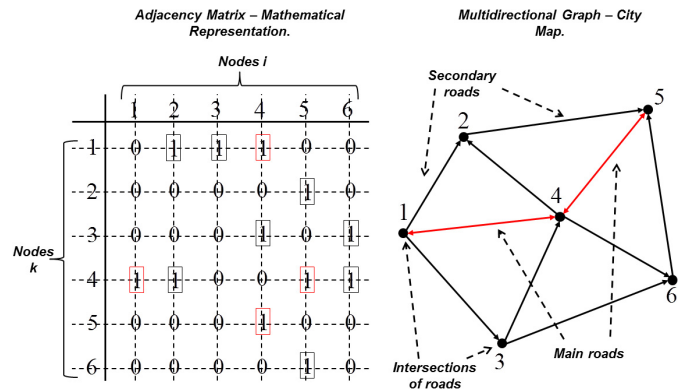


Fig. 1. Multidirectional graph and adjacency matrix.

II. MATHEMATICAL MODELING

In this section, the main hypotheses for the problem related to the charging infrastructure, delivery points, and so on are considered in detail. Moreover, the constraints related to the city map and the uncertainties in the navigation of the BEVs are taken into consideration.

A. Hypotheses

The following hypotheses are taken into account to address the problem.

- 1- A charging infrastructure exists on the city map.
- 2- The charging points located on the urban roads are known.
- 3- The delivery points located at the intersections of roads on the city map are known.
- 4- The BEV fleet and the charging infrastructure belong to the same owner.
- 5- The start and end points of the fleet are at the same place, called the warehouse.
- 6- The operator pre-schedules the deliveries assigned to each BEV, and these deliveries are made consecutively.
- 7- The batteries of the fleet begin with the same state of charge (SOC).
- 8- The charging rates differ according to the type of road: main (ultra-fast charging) or secondary (fast charging).

B. Modeling of the City Map

The city map, characterized by roads and their intersections, is modeled as a multidirectional graph and adjacency matrix [34]. Fig. 1 shows the adjacency matrix of rows and columns equal to the number of nodes (roads intersections) of this graph. The unit values represent the links between nodes k (starting node) and i (arrival node) that determine the element ki in the graph. Note that the bidirectional arrows (red) represent the main roads, while the unidirectional arrows (black) represent the secondary roads.

Also in Fig. 1 (right side), note that each main road is represented by two urban roads with opposite directions. The first main road (1,4) is represented by two unidirectional roads $1 \rightarrow 4$, and $4 \rightarrow 1$, and second road (4, 5) by $4 \rightarrow 5$, and $5 \rightarrow 4$. Moreover, these four unidirectional roads are elements (in the

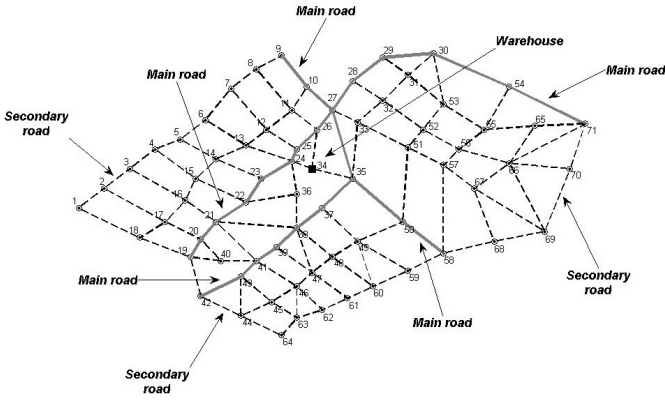


Fig. 2. City map contains 71 intersections and 131 urban roads.

red boxes) of the adjacency matrix (left side of Fig. 1). In this case, for each BEV vh , in delivery e , the variables $\omega_{vh,e,14}$, $\omega_{vh,e,41}$, $\omega_{vh,e,45}$, and $\omega_{vh,e,54}$ related with to main roads, will be selected depending on the location of the warehouse and the delivery point on the city map. Therefore, the variable $\omega_{vh,e,ki}$ identifies the main roads ki as unidirectional roads ki , and ik of the same length and number of the charging points, and with different directions. It is worth mentioning that, in the case of charging the BEV fleet batteries, it is the parameter t_{ki}^a , that allows the proposed model to differentiate the main and secondary roads according to the charging rate value.

Similar to the Fig. 1, each main road ki (gray lines) in Fig. 2 is represented by two unidirectional roads, allocated between nodes k and i , and in opposite directions $k \rightarrow i$, and $i \rightarrow k$. These main roads (in gray boxes) and secondary roads are shown in Table VII, in the Appendix, and contains the main characteristics of urban roads, such as the length, d_{ki} (km), and the number of charging points, n_{ki}^P . Furthermore, the charging points of the main and secondary roads differ according to their charging rates p_{ki}^{RU} , and according to the parameter, t_{ki}^a . For the main roads ($t_{ki}^a = 1$), the charging occurs at an ultra-fast rate, while the rate for the secondary roads ($t_{ki}^a = 0$) is considered fast; the black square located at intersection 34 stands for the warehouse of the BEV fleet.

C. Modeling the Uncertainties in Navigation

The uncertainties in the navigation for each BEV are represented by the influences of PTS, PS, and PPW in the urban roads ki . As a consequence of these influences, the delay times during navigation of the fleet are generated. Because these influences are a stochastic phenomenon, the use of random numbers in the modeling is necessary. These numerical values represent the occurrence probability of each of these influences on urban road ki . Therefore, the modeling of influences is important for determining the total delay time of each BEV during navigation on the city map.

To model the uncertainties PTS, PS, and PPW, a given horizon (a day) is taken into account. Therefore, the values of p_1 , p_2 , and p_3 , which stand for the probabilities of the BEV in each urban road ki of the city map for a specific day are determined randomly as shown in Fig. 3. As shown in Fig. 3, the occurrence of these uncertainties in each urban road ki are limited

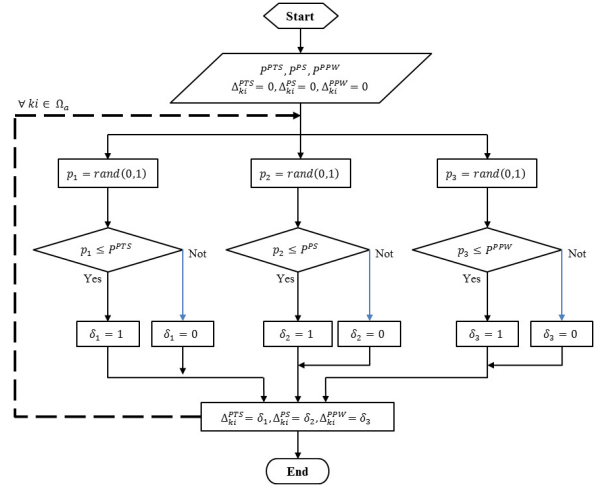


Fig. 3. Flowchart for the simulation of delay times.

by the values $PPTS$, PPS , and $PPPW$; in this paper these values are logically set to 0.5, 0.4, and 0.2, respectively [12]. Note that, PPW has the lowest probability of occurrence, because public works are not made for all urban roads in the city map; the delay time for PTS is more frequent to occur, especially in the city center, and nearby the crowded roads at the presence of more traffic lights, signs, etc. In the case of the presence of schools, basically, this probability represents the rush hours (opening and closing hours) existence of the building in the urban road ki . Therefore, in this paper each uncertainty (PTS , PS , and PPW) is modeled considering its probability of occurrence (p_1 , p_2 , and p_3) in each urban road ki in a specific day. Thus, this probability of occurrence determines the existence of a delay time during the navigation of the BEV through the urban road ki . These probabilities of occurrence are not determined (or calculated) for the specific periods in a day (e.g., each hour). It is worth mentioning that, considering the hourly operation of the BEV fleet would increase the model complexity and consequently results in decreasing the computational efficiency.

Aiming to determine the occurrence of delay times due to influences PTS, PS, and PPW on each urban road ki , an algorithm for modeling this stochastic phenomenon is proposed. Fig. 3 shows the flowchart of the simulating algorithm for the aforementioned uncertainties. The algorithm starts with established values $PPTS$, PPS , and $PPPW$, and the values Δ_{ki}^{PTS} , Δ_{ki}^{PS} , and Δ_{ki}^{PPW} initialized to zero. It is worth emphasizing that Δ_{ki}^{PTS} , Δ_{ki}^{PS} , and Δ_{ki}^{PPW} are the results of running the simulation algorithm, and they determine the occurrence of each influence PTS, PS, or PPW on urban road ki . Thus, these results are used as input data to the proposed model and complement the navigation and charging times in the constraint (15). Then, an iterative process is carried out for all urban roads ki . Thereafter, random values between zero and one are assigned to p_1 , p_2 , and p_3 . These random values are compared independently under the conditions $p_1 \leq PPTS$, $p_2 \leq PPS$, and $p_3 \leq PPPW$. Note that depending on the values p_1 , p_2 , and p_3 , the conditions can be true or false, and each urban road ki may present some, all, or none of the influences PTS, PS, and

PPW. Thus, if a condition is satisfied, then the corresponding δ (δ_1 to influence the PTS, δ_2 to influence the PS, and δ_3 to influence the PPW) takes 1, and otherwise, it takes 0.

It is worth mentioning that according to the number of satisfied conditions, for each urban road ki several cases can happen, such as: delay by influence PTS ($\delta_1 = 1$ and $\delta_2 = 0$ and $\delta_3 = 0$), delay by influences PS and PPW ($\delta_1 = 0$ and $\delta_2 = 1$ and $\delta_3 = 1$), or no influences ($\delta_1 = 0$ and $\delta_2 = 0$ and $\delta_3 = 0$). Thus, the values δ_1 , δ_2 , and δ_3 are attributed to Δ_k^{PTS} , Δ_{ki}^{PS} , and Δ_{ki}^{PPW} , respectively. These values are multiplied by their respective delay times, τ^{PTS} , τ^{PS} , and τ^{PPW} , established in the proposed model, as can be seen in (15).

III. THE PROPOSED MODEL

The proposed model is formulated initially as an MINLP problem, as (1)–(17). It is worth mentioning that the “ \forall ” in the equations stands for a “while”.

$$\text{Min } F \quad (1)$$

where F aims in the first case to minimize the costs for fleet maintenance (f_1) and in the second case to minimize the maintenance cost and costs related to the extra hours of the fleet of BEVs ($f_1 + f_2$). These functions are defined as follows.

$$f_1 = \delta^{km} \sum_{\forall vh \in \Omega_v} \sum_{\forall e \in \Omega_e} \sum_{\forall ki \in \Omega_a} d_{ki} \omega_{vh,e,ki}$$

$$f_2 = \delta^{hx} \sum_{\forall vh \in \Omega_v} \Delta t_{vh}$$

The constraints of this problem are considered in detail as follows.

$$\sum_{\forall ki \in \Omega_a} \omega_{vh,e,ki} - \sum_{\forall ij \in \Omega_a} \omega_{vh,e,ij} = -1 \quad \forall vh \in \Omega_v, \forall e \in \Omega_e$$

$$\forall i \in \Omega_n / t_{vh,e,i}^n = -1 \quad (2)$$

$$\sum_{\forall ki \in \Omega_a} \omega_{vh,e,ki} - \sum_{\forall ij \in \Omega_a} \omega_{vh,e,ij} = 0 \quad \forall vh \in \Omega_v, \forall e \in \Omega_e$$

$$\forall i \in \Omega_n / t_{vh,e,i}^n = 0 \quad (3)$$

$$\sum_{\forall ki \in \Omega_a} \omega_{vh,e,ki} - \sum_{\forall ij \in \Omega_a} \omega_{vh,e,ij} = 1 \quad \forall vh \in \Omega_v, \forall e \in \Omega_e$$

$$\forall i \in \Omega_n / t_{vh,e,i}^n = 1 \quad (4)$$

Constraints (2), (3), and (4) guarantee the determination of the shortest route for the navigation of BEV vh in delivery e . Constraint (2) is applied to obtain the shortest urban road d_{ij} to be traversed, starting from intersection i ($t_{vh,e,i}^n = -1$) for all possible intersections j . Fig. 4 illustrates an example related to constraint (2). Note that the intersection i ($t_{vh,e,i}^n = -1$) represents only the starting node to the intermediate nodes 1 ($t_{vh,e,1}^n = 0$), 2 ($t_{vh,e,2}^n = 0$), 3 ($t_{vh,e,3}^n = 0$), and 4 ($t_{vh,e,4}^n = 0$). Therefore, there is no BEV vh coming to the node i . Moreover, the red line (dashed) represents the shortest urban road d_{i2} to be traversed; this urban road $i2$ indicates the unit value of the variable $\omega_{vh,e,i2}$. Thus, the sum of the

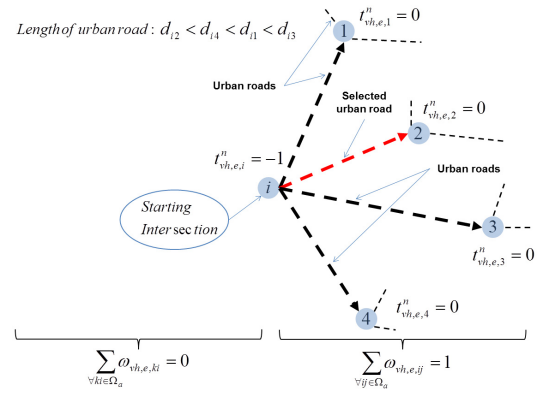


Fig. 4. Starting node BEV during navigation.

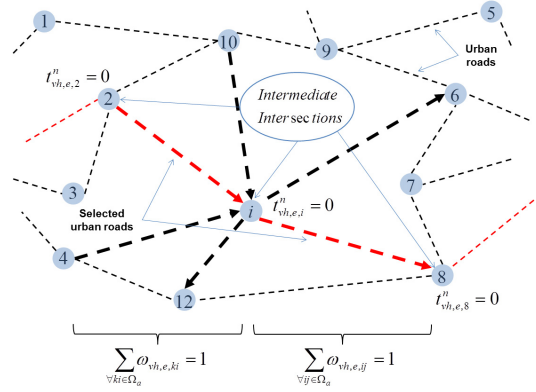


Fig. 5. Intermediate nodes BEV during navigation.

variables $\omega_{vh,e,ij}$ related to all possible urban roads ij results in 1.

The illustrative example of Fig. 5 is related to the constraint (3) and shows the navigation of BEV vh on urban roads formed with intermediate intersections, where the navigation from intersection k to i and from intersection i to j constitutes a minimum route ki and ij . In this case, the intermediate intersection i represents the arrival node for the BEV vh coming from the possible nodes 2 ($t_{vh,e,2}^n = 0$), 4 ($t_{vh,e,4}^n = 0$), and 10 ($t_{vh,e,10}^n = 0$) and at the same time it represents the starting node for the BEV vh going to the possible nodes 6 ($t_{vh,e,6}^n = 0$), 8 ($t_{vh,e,8}^n = 0$), and 12 ($t_{vh,e,12}^n = 0$). Thus, the sum of the variables $\omega_{vh,e,ki}$ related to the possible urban roads ki (intersections k with values 2, 4, and 10) results in 1 due to the selection of the shortest urban road $2i$. Similarly, the sum of the variables $\omega_{vh,e,ij}$ results in 1, (intersections j with values 6, 8, and 12) by selecting the shortest urban road $i8$.

In (4), the urban road ki is selected such that the length that must be traversed, starting from intermediate intersection k ($t_{vh,e,k}^n = 0$) to the possible arrival intersection i ($t_{vh,e,i}^n = 1$), is the shortest d_{ki} . Fig. 6 is used to illustrate constraint (4). Note that the intersection i represents only the arrival node and the intersections k are represented by intermediate nodes 2 ($t_{vh,e,2}^n = 0$), 6 ($t_{vh,e,6}^n = 0$), 7 ($t_{vh,e,7}^n = 0$), and 8 ($t_{vh,e,8}^n = 0$). Therefore, there exists no BEV vh starting from i to the other intermediate nodes. Here the red line (dashed) represents the

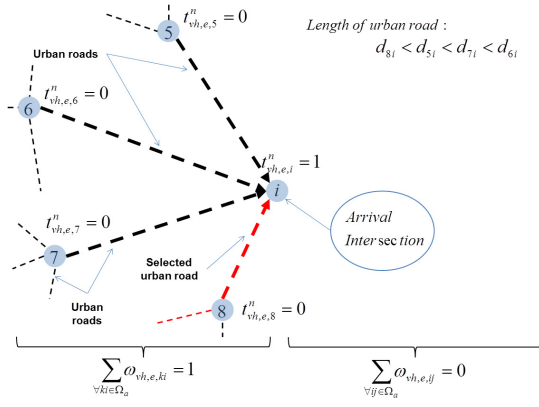


Fig. 6. Arrival node BEV during navigation.

shortest urban road $8i$ to be traversed, starting from all possible intersections k to the arrival intersection i ($t_{vh,e,i}^n = 1$). Thus, the sum of the variables $\omega_{vh,e,ki}$ related to the urban roads ki (intersection k with values 2, 6, 7, and 8) results in 1.

In order to initialize the state of charge SOC_{vh}^o of the BEV vh at intersection i ($t_{vh,e,i}^n = -1$) for the first delivery e , constraint (5) is considered. Note that the SOC is the state of energy available in the battery at a given moment.

$$SOC_{vh,e,i} = SOC_{vh}^o, \quad \forall vh \in \Omega_v, \forall e \in \Omega_e/e = 1, \\ \forall i \in \Omega_n/t_{vh,e,i}^n = -1 \quad (5)$$

The state of charge, $SOC_{vh,e-1,v}$, for the battery of BEV vh in delivery $e-1$ at intersection v ($t_{vh,e,v}^n = 1$) is equal to its state of charge in delivery e at intersection u ($t_{vh,e,u}^n = -1$), (6).

$$SOC_{vh,e,u} = SOC_{vh,e-1,v}, \quad \forall vh \in \Omega_v, \forall e \in \Omega_e, \forall u \in \Omega_n, \\ \forall v \in \Omega_n/t_{vh,e,u}^n = -1 \wedge t_{vh,e-1,v}^n = 1 \quad (6)$$

Fig. 7 shows an illustrative example related to constraints (5) and (6). Note that the arrows in red and blue represent the shortest routes to deliveries, $e = 1$ (intersection 4) and $e = 2$ (intersection 8) in their corresponding points. Constraint (5) is related to the initial state of charge of the BEV battery, $SOC_{vh,1,1}$, in the warehouse (starting at intersection 1 with $t_{vh,1,1}^n = -1$). This state of charge is represented by SOC_{vh}^o and is assigned to each BEV vh starting at intersection 1, towards the first delivery $e = 1$ (for this case, in arrival intersection 4 with $t_{vh,1,4}^n = 1$).

In order to explain constraint (6), in Fig. 7, node 4 is taken into consideration. Note that this node represents, for the shortest route in red ($e = 1$), the arrival intersection with $t_{vh,1,4}^n = 1$, and, for the shortest route in blue ($e = 2$), the starting intersection with $t_{vh,2,4}^n = -1$. Therefore, it is necessary to consider that for BEV vh , which existed in node 4, the state of charge of the first delivery ($SOC_{vh,1,4}$) should be equal to the state of charge of the second delivery ($SOC_{vh,2,4}$). In order to determine the state of charge of the battery for BEV vh , constraint (7), which contains two terms, including the available state of charge $SOC_{vh,e,i}^a$ and the charged energy $\varepsilon_{vh,e,ki}$ in urban road ki , is considered. Each SOC has its own limitations

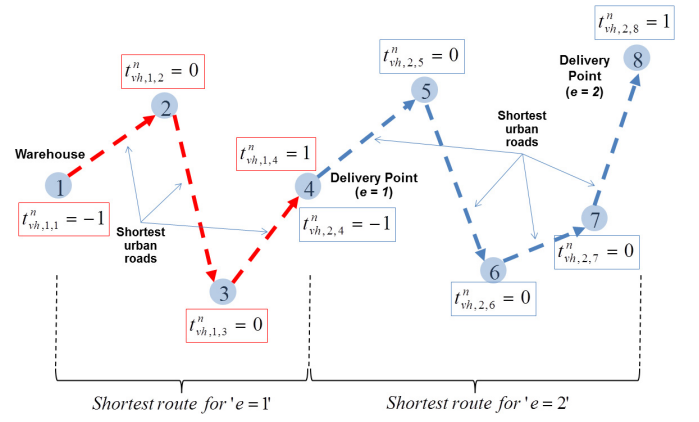


Fig. 7. Shortest route of each delivery in the city map.

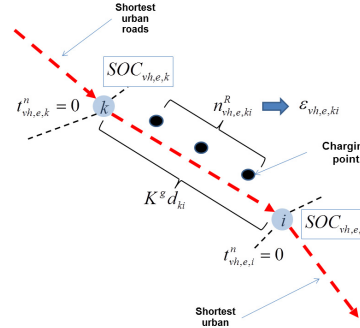


Fig. 8. BEV charging during navigation.

on energy storage in the fleet's batteries, represented in (8).

$$SOC_{vh,e,i} = SOC_{vh,e,i}^a + \sum_{\forall ki \in \Omega_a} \varepsilon_{vh,e,ki} \quad \forall vh \in \Omega_v, \forall e \in \Omega_e \\ \forall i \in \Omega_n/t_{vh,e,i}^n \geq 0 \quad (7) \\ 0.10 * K^s \leq SOC_{vh,e,i} \leq 0.98 * K^s \quad \forall vh \in \Omega_v, \forall e \in \Omega_e, \\ \forall i \in \Omega_n \quad (8)$$

$$SOC_{vh,e,i}^a = \sum_{\forall ki \in \Omega_a} \omega_{vh,e,ki} (SOC_{vh,e,k}^a - K^s d_{ki}) \quad \forall vh \in \Omega_v, \\ \forall e \in \Omega_e \forall i \in \Omega_n/t_{vh,e,i}^n \geq 0 \quad (9)$$

$$0 \leq SOC_{vh,e,i}^a, \quad \forall vh \in \Omega_v, \forall e \in \Omega_e, \\ \forall i \in \Omega_n/t_{vh,e,i}^n \geq 0 \quad (10)$$

In (9), the available energy in the battery $SOC_{vh,e,i}^a$ is calculated as the difference between the $SOC_{vh,e,k}^a$ at intersection k and $K^s d_{ki}$, which is the energy used during travel on urban road ki ($\omega_{vh,e,ki} = 1$). Finally, the non-negativity of $SOC_{vh,e,i}^a$ is guaranteed by (10) at intersection i with $t_{vh,e,i}^n \geq 0$. Fig. 8 illustrates in detail the concepts of constraints (7) and (9). Note that the shortest urban roads ki to be traversed are represented in red (dashed). Moreover, the variables $SOC_{vh,e,k}^a$ and $SOC_{vh,e,i}^a$ represent the state of charge of the BEV battery at the intermediate intersections k and i , respectively. Moreover, the number of charges, $n_{vh,e,ki}^R$, on urban road ki and the obtained energy, $\varepsilon_{vh,e,ki}$, by charging from these supply points

are shown. Constraint (7) considers the calculation of $SOC_{vh,e,i}$ of the battery BEV at the intermediate intersection i . This calculation takes into account the available energy, $SOC_{vh,e,i}^a$ and the energy to be recharged by BEV at charging points on the urban road ki , $\varepsilon_{vh,e,ki}$, is added to it. Moreover, the available energy in the intermediate intersection i , $SOC_{vh,e,i}^a$ is calculated via constraint (9) and considers the reduction of energy $K^g d_{ki}$ in addition to the state of charge $SOC_{vh,e,k}$ (at intermediate intersection k), as shown in Fig. 8.

$$\varepsilon_{vh,e,ki} = \omega_{vh,e,ki} n_{vh,e,ki}^R \tau_{vh,e,ki}^{RU} P_{ki}^{RU} \quad \forall vh \in \Omega_v \forall e \in \Omega_e, \quad \forall ki \in \Omega_a \quad (11)$$

$$\tau_{ki}^{MIN,UR} \leq \tau_{vh,e,ki}^{RU} \leq \tau_{ki}^{MAX,UR} \quad \forall vh \in \Omega_v \forall e \in \Omega_e \quad \forall ki \in \Omega_a / t_{ki}^a = 1 \quad (12)$$

$$\tau_{ki}^{MIN,R} \leq \tau_{vh,e,ki}^{RU} \leq \tau_{ki}^{MAX,R} \quad \forall vh \in \Omega_v \forall e \in \Omega_e \quad \forall ki \in \Omega_a / t_{ki}^a = 0 \quad (13)$$

$$0 \leq n_{vh,e,ki}^R \leq n_{ki}^P \quad \forall vh \in \Omega_v \forall e \in \Omega_e, \forall ki \in \Omega_a \quad (14)$$

The energy $\varepsilon_{vh,e,ki}$ is calculated by constraint (11), where the charging depends on $n_{vh,e,ki}^R$ and $\tau_{vh,e,ki}^{RU}$ at each point along urban road ki . By considering (12) and (13), the minimum and maximum $\tau_{vh,e,ki}^{RU}$ for urban road ki with $t_{ki}^a = 1$ and $t_{ki}^a = 0$ are guaranteed. In (14), the maximum number of charging points to be visited on urban road ki is guaranteed.

Finally, with constrain (15), the total time of operation of BEV vh considering the value t^{max} and extra hours Δt_{vh} to be penalized for the second case is determined in (1). Note that the total time of operation of BEV vh is composed of $\frac{d_{ki}}{v_{vh}^E}$, $\tau_{ki}^{PTS} \Delta_{ki}^{PTS}$, $\tau_{ki}^{PS} \Delta_{ki}^{PS}$, and $\tau_{ki}^{PPW} \Delta_{ki}^{PPW}$, which are the navigation times and delays due to PTS, PS, and PPW, respectively, and also the charging times $n_{vh,e,ki}^R \tau_{vh,e,ki}^{RU}$ for urban road ki chosen for the navigation of BEV vh . Constraints (16) and (17), respectively, stand for the main binary and integer decision variables $\omega_{vh,e,ki}$ and $n_{vh,e,ki}^R$.

$$\begin{aligned} & \sum_{\forall e \in \Omega_e} \sum_{\forall ki \in \Omega_a} \omega_{vh,e,ki} \left(\frac{d_{ki}}{v_{vh}^E} \right) \\ & + \sum_{\forall e \in \Omega_e} \sum_{\forall ki \in \Omega_a} \omega_{vh,e,ki} \left(\tau_{ki}^{PTS} \Delta_{ki}^{PTS} \right) \\ & + \sum_{\forall e \in \Omega_e} \sum_{\forall ki \in \Omega_a} \omega_{vh,e,ki} \left(\tau_{ki}^{PS} \Delta_{ki}^{PS} \right) \\ & + \sum_{\forall e \in \Omega_e} \sum_{\forall ki \in \Omega_a} \omega_{vh,e,ki} \left(\tau_{ki}^{PPW} \Delta_{ki}^{PPW} \right) \\ & + \sum_{\forall e \in \Omega_e} \sum_{\forall ki \in \Omega_a} \omega_{vh,e,ki} \left(n_{vh,e,ki}^R \tau_{vh,e,ki}^{RU} \right) \\ & \leq t^{max} + \Delta t_{vh} \quad \forall vh \in \Omega_v \quad (15) \end{aligned}$$

$$\omega_{vh,e,ki}; \text{ binary} \quad \forall vh \in \Omega_v, \forall e \in \Omega_e, \forall ki \in \Omega_a \quad (16)$$

$$n_{vh,e,ki}^R; \text{ integer} \quad \forall vh \in \Omega_v, \forall e \in \Omega_e, \forall ki \in \Omega_a. \quad (17)$$

A. Linearization

In the proposed model, a set of linearization procedures is applied to the non-linear constraints (9), (11), and (15). This set is inspired by the Big-M method [35]–[37], and is presented as linear constraints shown in Fig. 9. Note that these

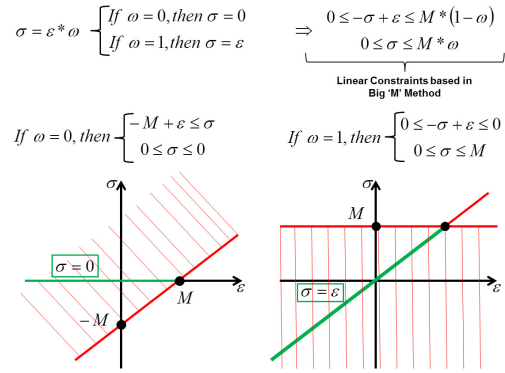


Fig. 9. Graphical representation of linear constraints.

non-linear constraints in the proposed model are related to the product of two variables; these variables are shown in Fig. 9 as ε (continuous variable) and ω (binary variable). When the product, σ , is evaluated for values of ω (0 or 1), σ results in 0 or ε , respectively. Therefore, a collection of linear constraints is necessary to obtain the same values of σ . Thus, the linear constraints shown in Fig. 9 are evaluated for the values of ω . If $\omega = 0$, then the resulting inequalities produce the set point $\sigma = 0$ (green line on the left side). Similarly, if $\omega = 1$, then the inequalities form the set of points $\sigma = \varepsilon$ (green line on the right side). Note that, defining a proper M is vital in the Big-M method and a large M may result in serious numerical difficulties on a computer, while a small M may not guarantee the optimal solution [38].

Using the linearization technique in [35], the following is the linear formulation for (9).

$$SOC_{vh,e,i}^a = \sum_{\forall ki \in \Omega_a} (\Delta''_{vh,e,ki} - K^g d_{ki} \omega_{vh,e,ki}) \quad \forall vh \in \Omega_v, \forall e \in \Omega_e \quad \forall i \in \Omega_n / t_{vh,e,i}^n \geq 0 \quad (18.a)$$

$$0 \leq -\Delta''_{vh,e,ki} + SOC_{vh,e,k} \quad \forall vh \in \Omega_v \forall e \in \Omega_e, \forall ki \in \Omega_a \quad (18.b)$$

$$-\Delta''_{vh,e,ki} + SOC_{vh,e,k} \leq M * (1 - \omega_{vh,e,ki}) \quad \forall ki \in \Omega_a \quad (18.c)$$

$$0 \leq \Delta''_{vh,e,ki} \quad \forall vh \in \Omega_v, \forall e \in \Omega_e, \forall ki \in \Omega_a \quad (18.d)$$

$$\Delta''_{vh,e,ki} \leq M * \omega_{vh,e,ki} \quad \forall vh \in \Omega_v, \forall e \in \Omega_e, \forall ki \in \Omega_a \quad (18.e)$$

To linearize constraint (11), $n_{vh,e,ki}^R$ is discretized with Y binary variables $W_{vh,e,ki,y}$ as in (19.b) and replaced in (19.a).

$$\varepsilon_{vh,e,ki} = P_{vh}^{RU} * \sum_{y=1}^Y \Delta Z_{vh,e,ki,y} \quad \forall vh \in \Omega_v \forall e \in \Omega_e \quad \forall ki \in \Omega_a \quad (19.a)$$

$$n_{vh,e,ki}^R = \sum_{y=1}^Y W_{vh,e,ki,y} \quad \forall vh \in \Omega_v, \forall e \in \Omega_e \quad \forall ki \in \Omega_a \quad (19.b)$$

$$0 \leq -\Delta W_{vh,e,ki,y} + \tau_{vh,e,ki}^{RU} \quad \forall vh \in \Omega_v, \forall e \in \Omega_e \quad \forall ki \in \Omega_a, \forall y = 1 \dots Y \quad (19.c)$$

$$\begin{aligned}
& -\Delta W_{vh,e,ki,y} + \tau_{vh,e,ki}^{RU} \quad \forall vh \in \Omega_v \forall e \in \Omega_e \\
& \leq M * (1 - W_{vh,e,ki,y}) \quad \forall ki \in \Omega_a, \forall y = 1 \dots Y \quad (19.d)
\end{aligned}$$

$$\begin{aligned}
0 \leq \Delta W_{vh,e,ki,y} \quad \forall vh \in \Omega_v, \forall e \in \Omega_e, \forall ki \in \Omega_a, \\
\forall y = 1 \dots Y \\
\forall vh \in \Omega_v, \forall e \in \Omega_e \quad (19.e)
\end{aligned}$$

$$\begin{aligned}
\Delta W_{vh,e,ki,y} \leq M * W_{vh,e,ki,y} \quad \forall ki \in \Omega_a, \forall y = 1 \dots Y \\
\forall vh \in \Omega_v, \forall e \in \Omega_e \quad (19.f)
\end{aligned}$$

$$\begin{aligned}
0 \leq -\Delta Z_{vh,e,ki,y} + \Delta W_{vh,e,ki,y} \quad \forall ki \in \Omega_a, \forall y = 1 \dots Y \\
\forall vh \in \Omega_v, \forall e \in \Omega_e \quad (19.g)
\end{aligned}$$

$$\begin{aligned}
-\Delta Z_{vh,e,ki,y} + \Delta W_{vh,e,ki,y} \quad \forall ki \in \Omega_a \\
\leq M * (1 - \omega_{vh,e,ki}) \quad \forall y = 1 \dots Y \quad (19.h)
\end{aligned}$$

$$\begin{aligned}
0 \leq \Delta Z_{vh,e,ki,y} \quad \forall vh \in \Omega_v, \forall e \in \Omega_e, \forall ki \in \Omega_a, \\
\forall y = 1 \dots Y \quad (19.i)
\end{aligned}$$

$$\begin{aligned}
\Delta Z_{vh,e,ki,y} \leq M * \omega_{vh,e,ki} \quad \forall vh \in \Omega_v, \forall e \in \Omega_e \\
\forall ki \in \Omega_a, \forall y = 1 \dots Y \quad (19.j)
\end{aligned}$$

By considering the linearization of (11), constraint (15) changes to the following form.

$$\begin{aligned}
& \sum_{\forall e \in \Omega_e} \sum_{\forall ki \in \Omega_a} \omega_{vh,e,ki} \left(\frac{d_{ki}}{v_{vh}^{VE}} \right) \\
& + \sum_{\forall e \in \Omega_e} \sum_{\forall ki \in \Omega_a} \omega_{vh,e,ki} \left(\tau^{PTS} \Delta_{ki}^{PTS} \right) \\
& + \sum_{\forall e \in \Omega_e} \sum_{\forall ki \in \Omega_a} \omega_{vh,e,ki} \left(\tau^{PS} \Delta_{ki}^{PS} \right) \\
& + \sum_{\forall e \in \Omega_e} \sum_{\forall ki \in \Omega_a} \omega_{vh,e,ki} \left(\tau^{PPW} \Delta_{ki}^{PPW} \right) \\
& + \sum_{\forall e \in \Omega_e} \sum_{\forall ki \in \Omega_a} \sum_{y=1}^Y \Delta Z_{vh,e,ki,y} \\
& \leq t^{max} + \Delta t_{vh} \quad \forall vh \in \Omega_v. \quad (20)
\end{aligned}$$

B. The MILP Model

The optimal route scheduling of the EVs for charging during navigation considering prespecified delivery points is modeled as an MILP problem as follows:

$$\min (1)$$

subject to: (1) – (7), (8), (10), (12) – (14), (16) – (20).

IV. TEST AND RESULTS

To evaluate the proposed MILP model, the system presented in Fig. 2 was used. In addition, the BEVs' batteries had a SOC_{vh}^o of 8.20 kWh, while their maximum capacity, K^s , was set to 30 kWh. Table I shows the deliveries e allocated to each BEV vh by the fleet operator.

In this paper, to implement and solve the proposed models, a modeling language for mathematical programming AMPL [39] and the commercial solver CPLEX [40] were used on a 2.67-GHz computer with 3 GB of RAM in order to guarantee that the optimal global solution would be found. The charging rates p_{ki}^{RU} were 6 kW (fast) and 10 kW (ultra-fast) for the main and secondary urban roads ki , respectively.

TABLE I
SCHEDULING OF DELIVERIES FROM STARTING POINT TO ARRIVAL POINT (STARTING→ARRIVAL) FOR BEVs

BEV	Delivery1	Delivery2	Delivery3	Delivery4	Return
1	34 → 25	25 → 10	10 → 7	7 → 5	5 → 34
2	34 → 22	22 → 2	2 → 19	19 → 41	41 → 34
3	34 → 38	38 → 50	50 → 61	61 → 46	46 → 34
4	34 → 29	29 → 51	51 → 68	68 → 60	60 → 34
5	34 → 33	33 → 57	57 → 65	65 → 70	70 → 34

TABLE II
SHORTEST ROUTE FOR BEV 1 DURING THE NAVIGATION

First Case	
Delivery 1	34 → 26 → 25
Delivery 2	25 → 12 → 11 → 10
Delivery 3	10 → 27 → 26 → 25 → 12 → 7
Delivery 4	7 → 8 → 11 → 26 → 25 → 24 → 23 → 14 → 5
Return	5 → 6 → 13 → 24 → 34
Second Case	
Delivery 1	34 → 26 → 25
Delivery 2	25 → 12 → 11 → 10
Delivery 3	10 → 27 → 26 → 25 → 12 → 7
Delivery 4	7 → 8 → 11 → 26 → 25 → 24 → 23 → 14 → 5
Return	5 → 6 → 13 → 24 → 34

TABLE III
SHORTEST ROUTE FOR BEV 2 DURING THE NAVIGATION

First Case	
Delivery 1	34 → 26 → 25 → 24 → 23 → 22
Delivery 2	22 → 21 → 20 → 19 → 18 → 1 → 2
Delivery 3	2 → 3 → 4 → 15 → 22 → 21 → 20 → 19
Delivery 4	19 → 40 → 41
Return	41 → 39 → 38 → 36 → 24 → 34
Second Case	
Delivery 1	34 → 26 → 25 → 24 → 23 → 22
Delivery 2	22 → 21 → 20 → 19 → 18 → 1 → 2
Delivery 3	2 → 3 → 4 → 15 → 22 → 21 → 20 → 19
Delivery 4	19 → 40 → 41
Return	41 → 39 → 38 → 36 → 24 → 34

The energy used during the navigation, K^8 , was 0.16 kWh/km, with an average speed of 40 km/h for each BEV [30]. Two cases were carried out, the first case to minimize the costs for fleet maintenance and the second case to minimize the maintenance cost and costs related to the extra hours of the fleet of BEVs.

The cost coefficients δ^{km} and δ^{hx} in (1) were in a ratio of 1 to 100, respectively, considering a greater weight for extra hours in the second case. In the operation of BEV vh , the time t^{max} was 8 hours (habitual working hours). In addition, the delay times for uncertainties τ^{PTS} , τ^{PS} , and τ^{PPW} were 1, 2, and 5 minutes, respectively [31].

Tables II, III, and IV show the shortest routes for BEVs 1, 2, and 3, respectively, in both cases. These tables represent the unit values of the binary variable, $\omega_{vh,e,ki}$ related to constraints (2), (3), and (4), as explained. An analysis done for BEV 1 is used as a descriptive example below. Thus, in delivery 1 of BEV 1, the proposed model determines the unit values of $\omega_{1,1,(34,26)}$ and $\omega_{1,1,(26,25)}$. These values indicate the BEV navigation by urban roads 34→26, and 26→25 or by shortest route 34→26→25 for both cases. Note that, in the first urban road 34→26, node 34 represents the warehouse, and

TABLE IV
SHORTEST ROUTE FOR BEV 3 DURING THE NAVIGATION

First Case	
Delivery 1	34 → 26 → 25 → 24 → 23 → 22 → 21 → 38
Delivery 2	38 → 37 → 35 → 33 → 51 → 50
Delivery 3	50 → 49 → 48 → 47 → 61
Delivery 4	61 → 62 → 46
Return	46 → 41 → 39 → 38 → 36 → 24 → 34
Second Case	
Delivery 1	34 → 26 → 25 → 24 → 23 → 22 → 21 → 38
Delivery 2	38 → 37 → 35 → 33 → 51 → 50
Delivery 3	50 → 49 → 59 → 60 → 61
Delivery 4	61 → 62 → 46
Return	46 → 41 → 39 → 38 → 36 → 24 → 34

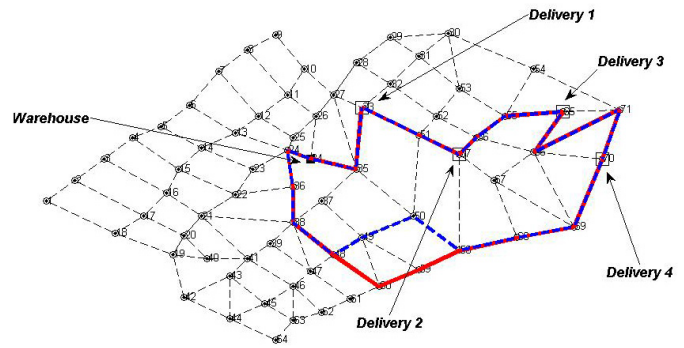


Fig. 11. Shortest route for BEV 5 during navigation.

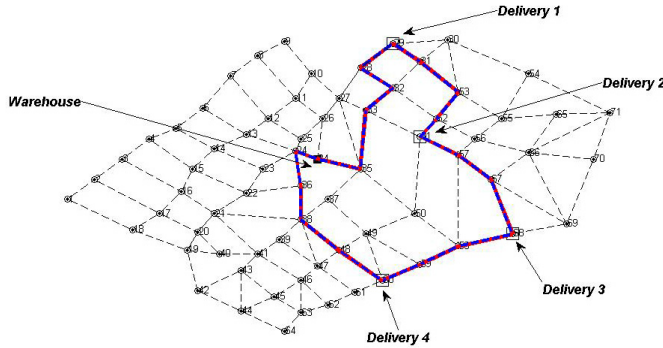


Fig. 10. Shortest route for BEV 4 during navigation.

in urban road 26→25, node 25 represents the delivery point 1 (BEV 1 arriving). In delivery 2, the variables with unit values a , $\omega_{1,2,(25,12)}$; $\omega_{1,2,(12,11)}$; and $\omega_{1,2,(11,10)}$, determine three urban roads ki to be traversed, such as: 25→12; 12→11; and 11→10 or the shortest route 25→12→11→10 for both cases. Note that, in this shortest route, nodes 25 and 10 represent delivery points 1 (BEV 1 starting) and 2 (BEV 1 arriving), respectively. In the case of delivery 3, the variables with unit value, $\omega_{1,3,(10,27)}$; $\omega_{1,3,(27,26)}$; $\omega_{1,3,(26,25)}$; $\omega_{1,3,(25,12)}$; and $\omega_{1,3,(12,7)}$, determine five urban roads, 10→27, 27→26, 26→25, 25→12, and 12→7 to be traversed for both cases. Moreover, the nodes 10 and 7 represent delivery points 2 (BEV 1 starting) and 3 (BEV 1 arriving), respectively. For the last delivery, the variables with unit value are $\omega_{1,4,(7,8)}$; $\omega_{1,4,(8,11)}$; $\omega_{1,4,(11,26)}$; $\omega_{1,4,(26,25)}$; $\omega_{1,4,(25,24)}$; $\omega_{1,4,(24,23)}$; $\omega_{1,4,(23,14)}$; and $\omega_{1,4,(14,5)}$, which determine the urban roads 7→8, 8→11, 11→26, 26→25, 25→24, 24→23, and 23→14, and 14→5 to be traversed in both cases. In this delivery, the nodes 7 and 5 represent delivery points 3 (BEV 1 starting) and 4 (BEV 1 arriving), respectively. Finally, in the return to the warehouse, the variables with unit values are $\omega_{1,5,(5,6)}$; $\omega_{1,5,(6,13)}$; $\omega_{1,5,(13,24)}$; and $\omega_{1,5,(24,34)}$, which determine the urban roads 5→6, 6→13, 13→24, and 24→34, to be traversed in both cases. Note that, the nodes 5 and 34 represent the delivery point 4 (BEV 1 starting) and the warehouse (BEV 1 arriving), respectively.

Thus, Table II shows the route of BEV 1 for each case. These routes coincided, resulting in a 153 km distance from the warehouse to delivery 4 and 39.3 km returning to the warehouse. A total operation time of 8h 37m 48s for the first case and 7h 58m 48s for the second case showed a reduction

of 22.3%. Note that the reduction was related to the total charging time of BEV 1. The shortest routes for BEV 2 in both cases are shown in Table III. Note that for both cases the routes coincided, presenting a total distance of 121 km from the warehouse to delivery 4 and 37.5 km returning to the warehouse. In addition, the total operating time for the first case was 7h 57m 36s, while for the second case it was 7h 15m 0s, which shows a total reduction of 8.9%. With coincident routes and an average speed of 40 km/h for the fleet, it can be concluded that this reduction was directly related to the total charging time for BEV 2.

Table IV shows the shortest route for BEV 3 for both cases. Note that the routes coincided minimally in both cases, because a change in the route of delivery 3 affected the navigation time. For the second case, this resulted in a reduction of the total navigation time of approximately 1.12% compared to the first case. Although for both cases the total distance of the shortest route was approximately 238 km, the total charging time of the second case showed a reduction of 36.9% compared to the first case, while the operating times of the first and second cases were 11h 56m 24s and 10h 6m 36s, respectively. Figs. 10 and 11 illustrate the shortest routes of BEVs 4 and 5, respectively, the first case in red and the second case in blue. In Fig. 10, for both cases, the shortest routes from the warehouse to delivery 4 and returning to the warehouse were 129 km and 60 km, respectively. The total operation time for the second case was 8h 3m 36s, which was about 27.08% less than the first case, which had a 9h 5m 24s operating time. This reduction is the result of different charging times during the navigation of BEV 4.

In Fig. 11, the change in the route (when returning to the warehouse) resulted in additional navigation time for the first case, about 0.78% more than the second case. Moreover, the charging time for the second case was reduced about 14.19%. Also, the total operating time for the first and second cases were 10h 51m 36s and 10h 16m 12s, respectively. For both cases, the shortest route was about 220 km. Finally, the shortest routes obtained for each BEV in the fleet, for both cases, demonstrate the effectiveness of the proposed model regarding operation times. An example of the effectiveness model in the reduction of operation times is demonstrated in the operation of BEVs 4 and 5. Note that the operating time of the BEVs and their components are analyzed in detail in Table V.

TABLE V
NAVIGATION, CHARGING, AND DELAY TIMES
IN THE OPERATION OF THE FLEET

BEV	Operation Time (h)		Navigation Time (h)		Charging Time (h)		Delay Time (h)
	First Case	Second Case	First Case	Second Case	First Case	Second Case	
	1	9.55	8.90	5.72	5.72	2.91	
2	9.05	8.34	5.09	5.09	2.87	2.16	1.09
3	13.08	11.25	7.20	7.12	4.74	2.99	1.14
4	9.76	8.73	5.41	5.41	3.68	2.65	0.67
5	11.72	11.13	6.35	6.40	4.51	3.87	0.86

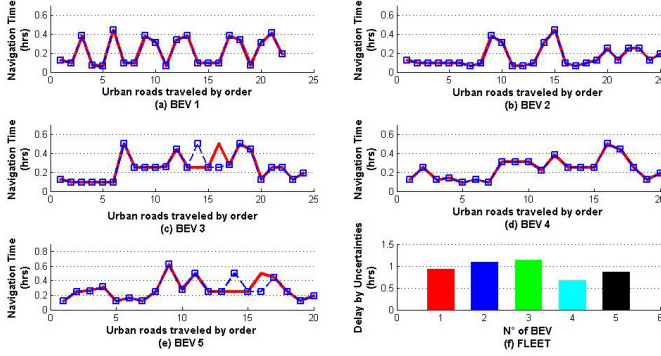


Fig. 12. Navigation times and delays due to the presence of an uncertainty.

Fig. 12 shows the total delay times for each BEV with uncertainty during navigation and the navigation times for urban roads ki traveled sequentially. Figs. 12 (a)–(c) illustrate the navigation times $\frac{d_{ki}}{v_{vh}^{VE}}$ for urban roads ki , presented in Tables II, III, and IV, respectively; red and blue lines stand for the first and second cases, respectively.

Note that in Figs. 12 (a) and (b), the coincident routes result in identical navigation times for both cases. For BEVs 1 and 2, the maximum navigation time (peak) was 24 minutes for urban roads ki with distances of approximately 17.5 km. Note that BEV 1 (with 6 peaks) presented a greater navigation time than BEV 2 (with 2 peaks). The navigation time with more peaks generates costs (related to extra hours) for the owner of the fleet. Fig. 12 (c) shows the variation in navigation times as a result of the change in urban roads on the route for delivery 3. The navigation time for these urban roads was 48 minutes for each case, with 30 km traveled. Note that as a result of the optimization process of the proposed model, both cases have the same number of peaks (maximum navigation time) with higher values at 24 minutes during navigation of BEV 3. Figs. 12 (d) and (e) show the navigation time for BEVs 4 and 5 for the routes illustrated in Figs. 10 and 11, respectively. Fig. 12 (d) shows identical navigation times in both cases for BEV 4 as a result of the coincident routes illustrated in Fig. 10. Furthermore, the maximum navigation time was 30 minutes on urban roads ki with 20 km traveled. Fig. 12 (e) shows the navigation time for BEV 5 for both cases resulting from the changes in urban roads ki occurring on the return route to the warehouse, as shown in Fig. 11. These urban roads changed by up to 40 km, and as a result, the navigation time increased by about 60 minutes. Note that in

TABLE VI
CHARGING TIMES, NUMBER OF CHARGES AND UNIT CHARGING
RATE FOR THE BEV 1 DURING NAVIGATION

Deliveries	Urban Road ki	BEV 1					
		First Case			Second Case		
		$\tau_{vh,e,ki}^{RU}$ (h)	$n_{vh,e,ki}^R$	p_{ki}^{RU} (kW)	$\tau_{vh,e,ki}^{RU}$ (h)	$n_{vh,e,ki}^R$	p_{ki}^{RU} (kW)
Delivery 1	34 → 26	0.00	0	0	0.00	0	0
	26 → 25	0.00	0	0	0.26	1	10
Delivery 2	25 → 12	0.00	0	0	0.00	0	0
	12 → 11	0.00	0	0	0.00	0	0
	11 → 10	0.00	0	0	0.00	0	0
Delivery 3	10 → 27	0.00	0	0	0.00	0	0
	27 → 26	0.28	1	10	0.00	0	0
	26 → 25	0.50	1	10	0.50	2	10
	25 → 12	0.00	0	0	0.00	0	0
	12 → 7	0.00	0	0	0.00	0	0
Delivery 4	7 → 8	0.00	0	0	0.00	0	0
	8 → 11	1.00	1	6	0.00	0	0
	11 → 26	0.00	0	0	0.00	0	0
	26 → 25	0.00	0	0	0.00	0	0
	25 → 24	0.00	0	0	0.50	2	10
	24 → 23	0.50	1	10	0.00	0	0
	23 → 14	0.00	0	0	0.00	0	0
	14 → 5	0.00	0	0	0.00	0	0
Return	5 → 6	0.00	0	0	0.00	0	0
	6 → 13	0.63	1	6	0.00	0	0
	13 → 24	0.00	0	0	0.00	0	0
	24 → 34	0.00	0	0	0.00	0	0

Figs. 12 (a)–(e), for each BEV, the number of peaks, and consequently the navigation times, are the same for both cases, as shown in Table V. Moreover, Fig. 12 (f) shows the delay times ($\tau_{PTS} + \tau_{PS} + \tau_{PPW}$) due to the presence of uncertainties during the operation of each BEV. It is observed that BEV 3 (green bar) and BEV 2 (blue bar) had the greatest delay times, greater than one hour, while BEV 4 showed the smallest delay time, approximately 0.7 hours. Finally, these results show the strong influence of uncertainties and the minimum navigation time to each BEV during operation and in the operation of the fleet. Table V shows the total operating time and its components for each BEV in the fleet. It was observed that the operating times and approximate navigation times for BEVs 3 and 5 were higher compared to the other BEVs. Note that there was a reduction in the charging time for the first case compared to the second case for both BEVs. Furthermore, BEV 3 had the highest delay time in the fleet due to the presence of uncertainties during navigation. Thus, after the optimization process, it is observed that charging times present a greater influence on the operation of BEVs.

Note that for BEV 2 and 3, the charging time component in the second case presents a significant reduction from the first case. This reduction is necessary (to minimize costs) due to the greater delay time from the presence of uncertainties during navigation. Therefore, optimization of the operation time results in reducing the charging time when the shortest route has higher delay times from the presence of uncertainties.

Table VI shows, for both cases, the recharging time for each charging point visited, the number of recharges, and the unit charging rate of BEV 1 on each urban road ki during

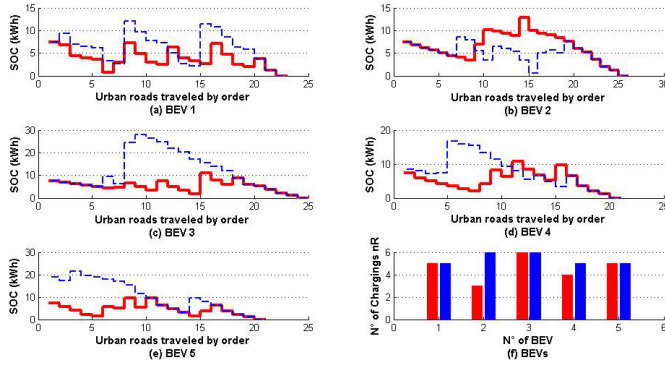


Fig. 13. Charge state and number of charges of the BEVs.

navigation. It is observed that in both cases BEV 1 presents the same total number of recharges after operation. Moreover, in the first case, only three recharges were ultra-fast (10 kW), and in the second case, all five recharges were ultra-fast. Note that in both cases, most of the recharges were made on urban roads ki belonging to deliveries 3 and 4. Total charging time after the operation of BEV 1 resulted in 2.91 and 2.26 hours for the first and second cases, respectively. Also, note that the lowest recharge time for the first case resulted in 0.28 hours (delivery 3), and 0.26 hours (delivery 1) in the second case. Finally, the results show a reduction of time of 0.65 hours in total recharge time for BEV 1. This reduction results in significant monetary terms when considering a large fleet.

Figs. 13 (a)–(e) show the profile of $SOC_{vh,e,i}$ for the BEVs for both cases, and Fig. 13 (f) shows the total number of charges, $\sum_{e \in \Omega_e} \sum_{ki \in \Omega_d} n_{vh,e,ki}^R$, for each BEV. In Fig. 13 (a), for the first case, BEV 1 shows five states of charge of 9.6% ($p_{ki}^{RU} = 10; n_{vh,e,ki}^R = 1$), 24.3% ($p_{ki}^{RU} = 10; n_{vh,e,ki}^R = 1$), 20.9% ($p_{ki}^{RU} = 6; n_{vh,e,ki}^R = 1$), 23.6% ($p_{ki}^{RU} = 10; n_{vh,e,ki}^R = 1$), and 12.7% ($p_{ki}^{RU} = 6; n_{vh,e,ki}^R = 1$) of K^s . For the second case, it shows three states of charge with values of 31.2% ($p_{ki}^{RU} = 10; n_{vh,e,ki}^R = 1$), 40.3% ($p_{ki}^{RU} = 10; n_{vh,e,ki}^R = 2$), and 38.3% ($p_{ki}^{RU} = 10; n_{vh,e,ki}^R = 2$). Note that, for both cases, more than 50% of the charging was ultra-fast. Thus, the shape of profile $SOC_{vh,e,i}$ for the second case shows the peak values of the stored energy in the battery of BEV 1 obtained with ultra-fast charging rates and reducing the charging time during operation. Note that, in the first case has more energy peaks (achieved with fast charging rates) than the second case, and these energy peaks are achieved with fast charging rates. For BEV 2 in the first case, Fig. 13 (b) shows three states of charge of 23.3% ($p_{ki}^{RU} = 6; n_{vh,e,ki}^R = 1$), 34.0% ($p_{ki}^{RU} = 6; n_{vh,e,ki}^R = 1$), and 42.7% ($p_{ki}^{RU} = 6; n_{vh,e,ki}^R = 1$) at the fast charging rate. In the second case, there are five states of charge of 28.3% ($p_{ki}^{RU} = 10; n_{vh,e,ki}^R = 1$), 21.3% ($p_{ki}^{RU} = 6; n_{vh,e,ki}^R = 1$), 17.0% ($p_{ki}^{RU} = 10; n_{vh,e,ki}^R = 2$), 19.0% ($p_{ki}^{RU} = 10; n_{vh,e,ki}^R = 1$), and 25.3% ($p_{ki}^{RU} = 6; n_{vh,e,ki}^R = 1$) at the ultra-fast rate for most of the time. Therefore, the second case shows an energy storage regime smaller than in the first case for most urban roads ki to be traversed. The energy stored values in the battery for the first case result of recharges with charging times near 1 hour.

In Fig. 13 (c), BEV 3 shows five states of charge, 15.0% ($p_{ki}^{RU} = 6; n_{vh,e,ki}^R = 1$), 21.6% ($p_{ki}^{RU} = 10; n_{vh,e,ki}^R = 1$), 25.3% ($p_{ki}^{RU} = 6; n_{vh,e,ki}^R = 1$), 36.7% ($p_{ki}^{RU} = 6; n_{vh,e,ki}^R = 2$), and 29.3% ($p_{ki}^{RU} = 6; n_{vh,e,ki}^R = 1$) along with the route in the first case. The second case shows three states of charge with values of 31.3% ($p_{ki}^{RU} = 10; n_{vh,e,ki}^R = 1$), 81.6% ($p_{ki}^{RU} = 10; n_{vh,e,ki}^R = 4$), and 92.9% ($p_{ki}^{RU} = 10; n_{vh,e,ki}^R = 1$) at the ultra-fast rate. Moreover, the profile $SOC_{vh,e,i}$ for the second case presents an energy peak close to the battery capacity. This peak presents the largest amount of charging in ultra-fast mode, with the charging times at approximately 30 minutes. After this peak, a new recharge is done at the same rate, providing the required energy to conclude the operation.

For BEV 4 in Fig. 13 (d), the obtained states of charge are, for the first case, 14.0% ($p_{ki}^{RU} = 6; n_{vh,e,ki}^R = 1$), 27.3% ($p_{ki}^{RU} = 6; n_{vh,e,ki}^R = 1$), 36.0% ($p_{ki}^{RU} = 6; n_{vh,e,ki}^R = 1$), and 32.0% ($p_{ki}^{RU} = 6; n_{vh,e,ki}^R = 1$), and for the second case, 55.8% ($p_{ki}^{RU} = 10; n_{vh,e,ki}^R = 2$), 21.3% ($p_{ki}^{RU} = 6; n_{vh,e,ki}^R = 1$), and 21.3% ($p_{ki}^{RU} = 6; n_{vh,e,ki}^R = 2$). Note that, the profile $SOC_{vh,e,i}$ in the second case presents the peak energy near about 50% of the battery capacity, and also in the first case the peaks are smaller and consecutive. In Fig. 13 (e) the states of charge for BEV 5 are, for the first case, 19.3% ($p_{ki}^{RU} = 6; n_{vh,e,ki}^R = 1$), 31.3% ($p_{ki}^{RU} = 6; n_{vh,e,ki}^R = 1$), 32.0% ($p_{ki}^{RU} = 6; n_{vh,e,ki}^R = 1$), 12.0% ($p_{ki}^{RU} = 6; n_{vh,e,ki}^R = 1$), and 21.3% ($p_{ki}^{RU} = 6; n_{vh,e,ki}^R = 1$), and for the second case 62.9% ($p_{ki}^{RU} = 6; n_{vh,e,ki}^R = 2$), 72.0% ($p_{ki}^{RU} = 6; n_{vh,e,ki}^R = 1$), and 32.0% ($p_{ki}^{RU} = 10; n_{vh,e,ki}^R = 2$). Thus, in the first case the BEV 5 begins without recharges and during navigation makes partial recharges less than 30% of battery capacity. In the second case the profile $SOC_{vh,e,i}$ of the BEV 5 after beginning operation stores energy with a peak value about 60% of the battery capacity. This stored energy peak value allows navigation of BEV 5 for more than half the shortest route determined by the proposed model.

Note that, the stored energy profile for each BEV shows the energy regime necessary for the attendance of all deliveries with the return to the warehouse in both cases. Fig. 13 (f) shows the total number of charges for the BEVs during navigation. Note that BEVs 1, 3, and 5 had an equal number of charges for both cases. Also, for BEVs 2 and 4, the number of charges in the second case was more than in the first case. Finally, the cost for the first case was approximately 4.46% higher than for the second case. Thus, it is evident that an optimization strategy for this problem should minimize the extra hours after working hours.

V. CONCLUSION

In this paper, an MILP model for optimizing the maintenance costs and extra hours in the route scheduling of a BEV fleet during the delivery of products at prespecified delivery points was proposed. The BEV on each route must have an efficient charging strategy. The proposed model considers a number of operational constraints related to the number of deliveries, average speed, location of delivery points, and charging, as well as the performance of the fleet's batteries.

TABLE VII
CHARGING POINTS AND LENGTH OF ROADS IN THE CITY MAP
WITH 71 INTERSECTIONS AND 131 URBAN ROADS

Urban Road (k,i)	d_{ki} (km)	n_{ki}^p	Urban Road (k,i)	d_{ki} (km)	n_{ki}^p	Urban Road (k,i)	d_{ki} (km)	n_{ki}^p
(1,2)	2.50	1	(27,28)	3.75	1	(49,48)	10.0	2
(2,3)	2.50	1	(27,33)	5.00	1	(49,59)	20.0	3
(3,4)	3.75	1	(27,35)	7.50	2	(50,35)	17.5	3
(4,5)	2.50	1	(28,29)	3.75	1	(50,49)	10.0	1
(4,15)	12.5	2	(29,31)	5.00	1	(51,50)	17.5	3
(5,6)	3.00	1	(29,30)	8.75	2	(51,57)	12.5	2
(6,7)	3.75	1	(30,53)	8.75	2	(52,32)	3.75	1
(6,13)	12.5	2	(30,54)	12.5	2	(52,51)	12.5	2
(7,8)	2.50	1	(31,30)	10.5	2	(53,52)	12.5	2
(8,9)	3.00	1	(31,53)	3.75	1	(53,55)	12.5	2
(8,11)	13.75	2	(32,28)	5.50	1	(54,71)	30.0	5
(9,10)	13.75	2	(32,31)	5.00	1	(55,54)	20.0	3
(10,27)	17.50	3	(33,32)	5.00	1	(55,65)	5.00	1
(11,10)	2.50	1	(33,51)	10.5	1	(56,55)	6.25	1
(11,26)	15.00	2	(34,35)	5.00	1	(56,52)	12.5	2
(12,11)	3.00	1	(34,26)	5.00	1	(57,56)	5.00	1
(12,7)	12.50	2	(35,33)	10.0	1	(57,67)	8.75	1
(13,12)	3.75	1	(36,22)	12.5	2	(58,57)	15.0	2
(13,24)	16.25	2	(36,24)	5.00	1	(58,50)	20.0	3
(14,13)	2.50	1	(37,35)	10.0	1	(58,59)	10.0	1
(14,5)	13.75	2	(37,49)	17.5	2	(59,60)	10.0	1
(15,14)	3.75	1	(38,36)	10.0	1	(60,49)	15.0	2
(15,22)	17.50	2	(38,37)	10.0	1	(60,48)	20.0	3
(16,15)	4.25	1	(38,47)	13.8	2	(60,61)	10.0	1
(16,3)	12.50	2	(39,38)	10.0	1	(61,62)	11.3	1
(17,16)	3.75	1	(39,47)	17.5	2	(62,46)	20.0	3
(17,20)	17.50	3	(40,20)	5.00	1	(62,63)	11.3	1
(18,17)	2.50	1	(40,41)	10.0	1	(63,46)	22.5	4
(18,1)	12.50	2	(41,21)	21.3	3	(63,64)	12.5	2
(19,40)	5.00	1	(41,39)	5.00	1	(64,44)	21.3	3
(19,18)	15.00	2	(42,19)	7.50	1	(65,66)	10.0	1
(20,19)	3.75	1	(42,43)	10.0	1	(66,56)	5.00	1
(21,20)	2.50	1	(43,41)	10.0	1	(66,67)	11.3	2
(21,38)	20.00	3	(43,44)	22.5	3	(66,71)	25.0	4
(21,16)	16.25	3	(43,45)	17.5	2	(67,68)	15.0	2
(22,21)	3.75	1	(44,42)	17.5	2	(67,69)	18.0	3
(23,14)	15.00	2	(45,44)	10.0	1	(68,58)	10.0	1
(23,22)	3.75	1	(45,63)	22.5	3	(69,68)	10.0	1
(24,23)	3.75	1	(46,41)	17.5	3	(69,66)	25.0	4
(24,34)	7.50	1	(46,45)	10.0	1	(70,66)	22.5	4
(25,24)	3.75	1	(47,46)	10.0	1	(70,69)	20.0	3
(25,12)	15.00	2	(47,61)	20.0	3	(71,70)	11.3	1
(26,25)	3.75	1	(48,38)	17.5	2	(71,65)	12.5	2
(27,26)	3.75	1	(48,47)	10.0	1	-	-	-

The uncertainties are modeled using the probability of delays due to the PTS, PS, and PPW. A city map with 71 intersections and 131 urban roads, main and secondary, was used. Results showed that considering the extra hours due to the presence of uncertainties resulted in the optimal scheduling of BEVs with the minimum cost. The proposed model is a useful tool in the analysis, evaluation, and planning of the economic operation of BEVs, encouraging companies to use this transport technology in the areas of services, thereby ensuring sustainability and, as a byproduct, reducing pollution in urban areas.

APPENDIX

The Table VII contains the data related to the city map.

REFERENCES

[1] M. Brenna, F. Foiadelli, and D. Zaninelli, "Integration of recharging infrastructures for electric vehicles in urban transportation system," in *Proc. IEEE Int. Energy Conf. Exhibit. (ENERGYCON)*, Florence, Italy, Sep. 2012, pp. 1060–1064.

[2] M. A. Rahman, Q. Duan, and E. Al-Shaer, "Energy efficient navigation management for hybrid electric vehicles on highways," in *Proc. ACM/IEEE Int. Conf. Cyber-Phys. Syst. (ICCCPS)*, Philadelphia, PA, USA, Apr. 2013, pp. 21–30.

[3] S. Sachan and N. Kishor, "Optimal location for centralized charging of electric vehicle in distribution network," in *Proc. 18th Mediterr. Electrotech. Conf. (MELECON)*, Limassol, Cyprus, Apr. 2016, pp. 1–6.

[4] L. Jia, Z. Hu, W. Liang, W. Lang, and Y. Song, "A novel approach for urban electric vehicle charging facility planning considering combination of slow and fast charging," in *Proc. Int. Conf. Power Syst. Technol. (POWERCOM)*, Chengdu, China, Oct. 2014, pp. 3354–3360.

[5] R.-C. Leou, "Optimal charging/discharging control for electric vehicles considering power system constraints and operation costs," *IEEE Trans. Power Syst.*, vol. 31, no. 3, pp. 1854–1860, May 2016.

[6] Y. Tang, J. Zhong, and M. Bollen, "Aggregated optimal charging and vehicle-to-grid control for electric vehicles under large electric vehicle population," *IET Gener. Transm. Distrib.*, vol. 10, no. 8, pp. 2012–2018, May 2016.

[7] S. Falahati, S. A. Taher, and M. Shahidehpour, "A new smart charging method for EVs for frequency control of smart grid," *Int. J. Elect. Power Energy Syst.*, vol. 83, pp. 458–469, Dec. 2016.

[8] X. Jin, K. Li, and A. I. Sivakumar, "Scheduling and optimal delivery time quotation for customers with time sensitive demand," *Int. J. Prod. Econ.*, vol. 145, no. 1, pp. 349–358, Sep. 2013.

[9] D. Xue, H. Wang, and D. H. Norrie, "A fuzzy mathematics based optimal delivery scheduling approach," *Comput. Ind.*, vol. 45, no. 3, pp. 245–259, Jul. 2001.

[10] G. Wang and A. Gunasekaran, "Operations scheduling in reverse supply chains: Identical demand and delivery deadlines," *Int. J. Prod. Econ.*, vol. 183, pp. 375–381, Jan. 2017. [Online]. Available: <http://dx.doi.org/10.1016/j.ijpe.2016.08.010>

[11] Y. Yu, J. Tang, J. Li, W. Sun, and J. Wang, "Reducing carbon emission of pickup and delivery using integrated scheduling," *Transp. Res. D Transp. Environ.*, vol. 47, pp. 237–250, Aug. 2016.

[12] S. Kim, M. E. Lewis, and C. C. White, "Optimal vehicle routing with real-time traffic information," *IEEE Trans. Intell. Transp. Syst.*, vol. 6, no. 2, pp. 178–188, Jun. 2005.

[13] T. Jurik *et al.*, "Energy optimal real-time navigation system," *IEEE Intell. Transp. Syst. Mag.*, vol. 6, no. 3, pp. 66–79, Jul. 2014.

[14] T. M. Sweda and D. Klabjan, "Finding minimum-cost paths for electric vehicles," in *Proc. IEEE Int. Elect. Veh. Conf. (IEVC)*, Greenville, SC, USA, Mar. 2012, pp. 1–4.

[15] S. Pourazam, C. G. Cassandras, and A. Malikopoulos, "Optimal routing of electric vehicles in networks with charging nodes: A dynamic programming approach," in *Proc. IEEE Int. Elect. Veh. Conf. (IEVC)*, Florence, Italy, Dec. 2014, pp. 1–7.

[16] F. Alesiani and N. Maslekar, "Optimization of charging stops for fleet of electric vehicles: A genetic approach," *IEEE Intell. Transp. Syst. Mag.*, vol. 6, no. 3, pp. 10–21, Jul. 2014.

[17] S. Chang, H. Li, and K. Nahrstedt, "Charging facility planning for electric vehicles," in *Proc. IEEE Int. Elect. Veh. Conf. (IEVC)*, Florence, Italy, Dec. 2014, pp. 1–7.

[18] K. Villez, A. Gupta, V. Venkatasubramanian, and C. Rieger, "Resilient design of recharging station networks for electric transportation vehicles," in *Proc. 4th Int. Symp. Resilient Control Syst. (ISRCRS)*, Boise, ID, USA, Aug. 2011, pp. 55–60.

[19] M. Brenna, F. Foiadelli, and D. Zaninelli, "Power and energy estimation for plug-in electric vehicles recharge in metropolitan area," in *Proc. 11th Int. Conf. Elect. Power Qual. Utilisation (EPQU)*, Lisbon, Portugal, Oct. 2011, pp. 1–6.

[20] J. Kirby and F. Hassan, "AC recharging infrastructure for EVs and future smart grids—A review," in *Proc. 47th Int. Univ. Power Eng. Conf. (UPEC)*, London, U.K., Sep. 2012, pp. 1–6.

[21] C. Rottondi, G. Neglia, and G. Verticale, "Complexity analysis of optimal recharge scheduling for electric vehicles," *IEEE Trans. Veh. Technol.*, vol. 65, no. 6, pp. 4106–4117, Jun. 2016.

[22] C. Rottondi, G. Verticale, and G. Neglia, "On the complexity of optimal electric vehicles recharge scheduling," in *Proc. IEEE Online Conf. Green Commun. (OnlineGreenComm)*, Tucson, AZ, USA, Nov. 2014, pp. 1–7.

[23] Y. D. Ko and Y. J. Jang, "The optimal system design of the online electric vehicle utilizing wireless power transmission technology," *IEEE Trans. Intell. Transp. Syst.*, vol. 14, no. 3, pp. 1255–1265, Sep. 2013.

[24] L. Feng, S. Ge, H. Liu, L. Wang, and Y. Feng, "The planning of charging stations on the urban trunk road," in *Proc. IEEE-PES Innov. Smart Grid Technol. Asia (ISGT Asia)*, Tianjin, China, May 2012, pp. 1–4.

- [25] A. Y. S. Lam, Y.-W. Leung, and X. Chu, "Electric vehicle charging station placement: Formulation, complexity, and solution," *IEEE Trans. Smart Grid*, vol. 5, no. 6, pp. 2846–2856, Nov. 2014.
- [26] J. Timpner and L. Wolf, "Design and evaluation of charging station scheduling strategies for electric vehicles," *IEEE Trans. Intell. Transp. Syst.*, vol. 15, no. 2, pp. 579–588, Apr. 2014.
- [27] E. Yudovina and G. Michailidis, "Socially optimal charging strategies for electric vehicles," *IEEE Trans. Autom. Control*, vol. 60, no. 3, pp. 837–842, Mar. 2015.
- [28] I. S. Bayram, G. Michailidis, M. Devetsikiotis, and F. Granelli, "Electric power allocation in a network of fast charging stations," *IEEE J. Sel. Areas Commun.*, vol. 31, no. 7, pp. 1235–1246, Jul. 2013.
- [29] C. Jin, J. Tang, and P. Ghosh, "Optimizing electric vehicle charging: A customer's perspective," *IEEE Trans. Veh. Technol.*, vol. 62, no. 7, pp. 2919–2927, Sep. 2013.
- [30] T. Ma and O. A. Mohammed, "Optimal charging of plug-in electric vehicles for a car-park infrastructure," *IEEE Trans. Ind. Appl.*, vol. 50, no. 4, pp. 2323–2330, Jul./Aug. 2014.
- [31] Y. He, B. Venkatesh, and L. Guan, "Optimal scheduling for charging and discharging of electric vehicles," *IEEE Trans. Smart Grid*, vol. 3, no. 3, pp. 1095–1105, Sep. 2012.
- [32] C. Chen and S. Duan, "Optimal integration of plug-in hybrid electric vehicles in microgrids," *IEEE Trans. Ind. Informat.*, vol. 10, no. 3, pp. 1917–1926, Aug. 2014.
- [33] K. Lee, *Modern Heuristic Optimization Techniques With Applications to Power Systems*. New York, NY, USA: Wiley, 2005.
- [34] B. Andrasfai, *Graph Theory: Flows, Matrices*. New York, NY, USA: Taylor & Francis, 1991.
- [35] I. S. Kourtev, B. Taskin, and E. G. Friedman, *Timing Optimization Through Clock Skew Scheduling*. New York, NY, USA: Springer, 2009.
- [36] H. S. Kasana and K. D. Kumar, *Introductory Operations Research*. Heidelberg, Germany: Springer, 2004.
- [37] P. S. Iyer, *Operations Research*. New Delhi, India: Tata McGraw Hill, 2009.
- [38] M. Pourakbari-Kasmaei, M. J. Rider, and J. R. S. Mantovani, "An unambiguous distance-based MIQP model to solve economic dispatch problems with disjoint operating zones," *IEEE Trans. Power Syst.*, vol. 31, no. 1, pp. 825–826, Jan. 2016.
- [39] R. Fourer, D. M. Gay, and B. W. Kernighan, *AMPL: A Modeling Language for Mathematical Programming*, 2nd ed. Pacific Grove, CA, USA: Brooks/Cole, 2003.
- [40] *Optimization Subroutine Library Guide and Reference, Version 11.0, Incline*, CPLEX Div., Village, NV, USA, and ILOG Inc., Sunnyvale, CA, USA, 2008.

Fernando V. Cerna received the B.Sc. degree in electrical engineering from the Universidad Nacional del Callao, Lima, Peru, in 2008, and the M.Sc. and Ph.D. degrees in electrical engineering from São Paulo State University, Ilha Solteira, Brazil, in 2013 and 2017, respectively. His research interests include development of methodologies for the optimization, planning, and control of electrical power distribution systems.

Mahdi Pourakbari-Kasmaei (S'10–M'15) received the B.Sc. degree in electrical engineering from the LIAU, Guilan, Iran, in 2005, the M.Sc. degree in electrical engineering from the Shahid Bahonar University of Kerman, Kerman, Iran, in 2008, and the Ph.D. degree in electrical engineering from the Universidade Estadual Paulista (UNESP), Ilha Solteira, Brazil, in 2015. He was a Consultant in a power distribution company and the Project Executive in three practical projects. He is a Post-Doctoral Researcher with UNESP and currently a Visiting Researcher with the University of Castilla-La Mancha, Ciudad Real, Spain. His research interests include power systems planning, operations and economics, and environmental issues.

Rubén A. Romero (SM'08) received the B.Sc. and P.E. degrees from the National University of Engineering, Lima, Peru, in 1978 and 1984, respectively, and the M.Sc. and Ph.D. degrees from the Universidade Estadual de Campinas, Campinas, Brazil, in 1990 and 1993, respectively. He is currently a Professor of Electrical Engineering with the Universidade Estadual Paulista Julio de Mesquita Filho, Ilha Solteira, Brazil. His research interests include methodologies for the optimization, planning, and control of electrical power systems, applications of artificial intelligence in power system, and operations research.

Marcos J. Rider (S'97–M'06–SM'16) received the B.Sc. (Hons.) and P.E. degrees from the National University of Engineering, Lima, Peru, in 1999 and 2000, respectively, the M.Sc. degree from the Federal University of Maranhão, Maranhão, Brazil, in 2002, and the Ph.D. degree from the University of Campinas, Campinas, Brazil, in 2006, all in electrical engineering, where he is currently a Professor with the Department of Systems and Energy. His areas of research are the development of methodologies for the optimization, planning, and control of electrical power systems, and applications of artificial intelligence in power systems.